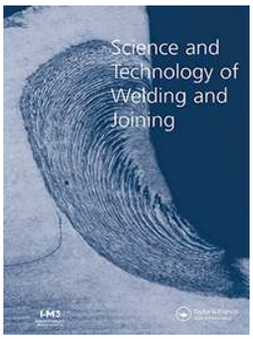

Science and Technology of Welding and Joining

ISSN: (Print) (Online) Journal homepage: www.tandfonline.com/journals/ystw20

Test for stress relief cracking susceptibility in creep resistant chromium-molybdenum steels

Conner Sarich, Boian Alexandrov, Avraham Benatar & Jorge Penso

To cite this article: Conner Sarich, Boian Alexandrov, Avraham Benatar & Jorge Penso (2022) Test for stress relief cracking susceptibility in creep resistant chromium-molybdenum steels, Science and Technology of Welding and Joining, 27:4, 265-281, DOI: 10.1080/13621718.2022.2050133

To link to this article: https://doi.org/10.1080/13621718.2022.2050133

Published online: 16 Mar 2022.

SCIENCE AND TECHNOLOGY OF WELDING AND JOINING
2022, VOL. 27, NO. 4, 265–281
https://doi.org/10.1080/13621718.2022.2050133

I·M3 Institute of Materials, Minerals & Mining
Taylor & Francis Taylor & Francis Group

Test for stress relief cracking susceptibility in creep resistant chromium-molybdenum steels

Conner Sarich[a], Boian Alexandrov[a], Avraham Benatar[a] and Jorge Penso[b]

[a]Welding Engineering Program, Department of Materials Science and Engineering, The Ohio State University, Columbus, OH, USA; [b]Shell Global Solutions US Inc., Houston, TX, USA

ABSTRACT

An externally restrained stress relief cracking test was developed and demonstrated in testing susceptible and resistant to cracking welds in Cr–Mo steels. Compared to other externally restrained tests, it simultaneously applies stress and compensates thermal expansion during heating to post-weld heat treatment temperature and utilises digital image correlation for quantification of key characteristics of the stress relaxation and stress relief cracking phenomena. In contrast with resistant to stress relief cracking materials, susceptible materials experienced lower levels of stress relaxation, strain absorption, and sustained mechanical energy, with accelerated kinetics of strain accumulation and strain localisation leading to failure. The processes of stress relief cracking and stress relaxation were quantified as low strain – slow strain rate – low energy phenomena.

ARTICLE HISTORY
Received 2 December 2021
Revised 18 February 2022
Accepted 20 February 2022

KEYWORDS
Stress relief cracking test; Cr–Mo steels; stress relaxation; strain concentration; strain rate; sustained mechanical energy

Introduction

Stress relief cracking (SRC) has been extensively studied to gain a better understanding of the cracking mechanism and to determine susceptible materials [1,2]. SRC occurs during post-weld heat treatment (PWHT) in highly restrained thick-walled welds that build up high residual stresses during welding. In Cr–Mo steels, SRC occurs when grain interiors are strengthened by carbide reprecipitation during PWHT, leading to grain boundary strain accumulation and cracking during the stress-relieving process. Several theories about the SRC mechanism have been proposed which correlate grain interior strengthening and grain boundary embrittling to cracking [3–6]. There are multiple variables that can impact the likelihood of SRC such as composition, welding process/procedure, residual stress level, weld restraint, and PWHT procedure [2].

Refabricating, repair, and operational downtime are costly consequences of SRC, making the elimination of SRC occurrences highly financially incentivized. Improving the understanding of the mechanisms for SRC and reliable prediction of the cracking susceptibility are two ways that SRC susceptibility can be reduced or eliminated during fabrication. A range of tests aiming at recreating the SRC mechanism and evaluating cracking susceptibility in welds of creep-resistant steels have been developed and implemented. The main features for a few SRC tests, related to replicating the conditions for SRC in highly restrained, high residual stress welds, are summarised in Table 1.

Based on the loading conditions, the SRC tests can be classified as self-restrained, strain to failure, and externally restrained. The Notched C-Ring test [7] and the University of Pennsylvania test [8] are self-restrained. Both utilise notched samples that are preloaded with tensile stresses in bending devices and subjected to PWHT. Relative cracking susceptibility in tested materials is ranked by the presence or absence of cracks in front of the notch at a particular level of preloading. The level of restraint in these tests varies during testing, depending on the design and thermal expansion of the loading devices and tested samples and may not accurately reproduce the conditions leading to SRC in highly restrained welds.

The Belgian Welding Institute (BWI) test [9] and the standardised American Petroleum Institute (API) test [10] are strain to failure tests. Both tests involve straining of test samples, during holding at PWHT temperature, with a constant, slow extension rate until failure. These tests provide a relative ranking of cracking susceptibility based on reduction in area (RA) in tested samples. However, due to unloaded heating to PWHT temperature, short exposure at PWHT, and continuous tensile displacement, these cannot accurately replicate the carbide precipitation and stress relaxation mechanisms leading to SRC in highly restrained welds.

Three externally restrained SRC tests have been developed utilising the Gleble™ thermo-mechanical simulator (Table 1). These tests simulate coarse grain heat-affected zone (CGHAZ) and PWHT thermal

CONTACT Boian Alexandrov alexandrov.1@osu.edu Welding Engineering Program, Department of Materials Science and Engineering, The Ohio State University, 1248 Arthur E. Adams Drive, Columbus, OH 43221, USA

Table 1. Main features of SRC tests.

Loading type	Test	Test sample	Welding residual stresses	PWHT thermal history	Stress relaxation under high restraint	Susceptibility quantification	Advantages
Self-restrained	Notched C-Ring [8]	Weld	Yes	Yes	Close	Limited: presence of cracks	Multi-axial stress
	Pennsylvania University [9]	Simulated HAZ	Yes	Yes	Close		
Strain to failure	BWI [10]	Simulated HAZ	No	No	No	Limited: RA	Short testing time
	API [11]	Weld	No	No	No		
Externally restrained	Lehigh 2000 [12]	Simulated HAZ	Yes	Yes	Close	Failure time, failure stress, RA	High process control
	OSU 2014 [13]		Yes	Yes	Close		
	Lehigh 2019 [14]		No	Yes	Yes		

histories on test samples and involve different mechanical loading procedures for simulation of welding residual stresses and stress relaxation. The Lehigh 2000 test [11] applies a gradually increasing tensile load on cooling in the CGHAZ simulation. The final load is in the order of the tested material yield strength at the selected PWHT temperature. The load is held constant during the PWHT simulation, which does not fully replicate the conditions of stress relaxation under high restraint. The OSU 2014 test [12] applies tensile load equal to 90% of the material yield strength after the CGHAZ simulation. The sample is then held under fixed displacement during the PWHT simulation to closely replicate stress relief in highly restrained welds. However, thermal expansion of the test sample on heating to PWHT temperature may result in significant stress reduction before the onset of the PWHT. The Lehigh 2019 test [13] applies 0.2% offset stress at reaching the PWHT temperature and holds the test under fixed displacement for the test duration. This loading procedure does not reproduce the effect of welding residual stresses on carbide precipitation during heating to PWHT temperature. The externally restrained tests quantify SRC susceptibility by time to failure, stress at failure, strain at failure (OSU 2014), and RA.

The performed comparative analysis shows that self-restrained and externally restrained tests better replicate the SRC mechanism than the strain to failure tests (Table 1). The externally restrained tests also better quantify the SRC susceptibility and provide a higher degree of process control. However, none of the existing tests can fully reproduce the conditions leading to SRC in highly restrained, high residual stress welds.

The objective of this work was to develop and demonstrate an externally restrained test that closely reproduces the mechanism of SRC during PWHT of highly restrained, high residual stress thick-walled weldments and generates quantifiable characteristics of the stress relief process and SRC susceptibility. The approach for test development, the test demonstration and validation by quantifying the stress relief mechanism in SRC susceptible and resistant materials, and a direct comparison to a standardised, industry used SRC test will be covered.

Test development, materials and procedure

OSU SRC test development

The first step taken for SRC test development was to identify essential stress, strain, and temperature characteristics of weldments that are necessary to recreate the microstructural evolution leading up to cracking, as well as recreate the SRC mechanism as it would occur in weldments during PWHT. Three key components of the SRC mechanism were incorporated in the SRC testing procedure: (1) welding thermal histories that generate microstructures susceptible to SRC, (2) high welding residual stresses that would require stress-relieving PWHT, and (3) high restraint that leads to SRC in the process of stress-relieving during PWHT.

The SRC testing procedure utilises the Gleeble™ thermo-mechanical simulator, which is capable of accurately recreating welding and PWHT thermal histories and simulating welding residual stresses and high weld restraint. A schematic of the SRC testing procedure is shown in Figure 1. It is based on the OSU 2014 SRC test [12] and introduces (1) compensation for stress relaxation due to test sample thermal expansion on heating to PWHT temperature, (2) quantification of the kinetics of local strain accumulation caused by stress relaxation, and (3) quantification of the level of stress relief in SRC resistant materials.

As an initial step, a HAZ thermal history is simulated on a sample from the tested material. This step is optional in the case of testing actual weldments. Next, the test sample is loaded to 90% of the tested material yield strength, aiming to simulate a high level of welding residual stress. This is followed by heating at a rate of 200°C h^{-1} to the desired PWHT temperature. Simultaneously, the test sample is strained at a constant stroke rate to achieve a predetermined tensile load

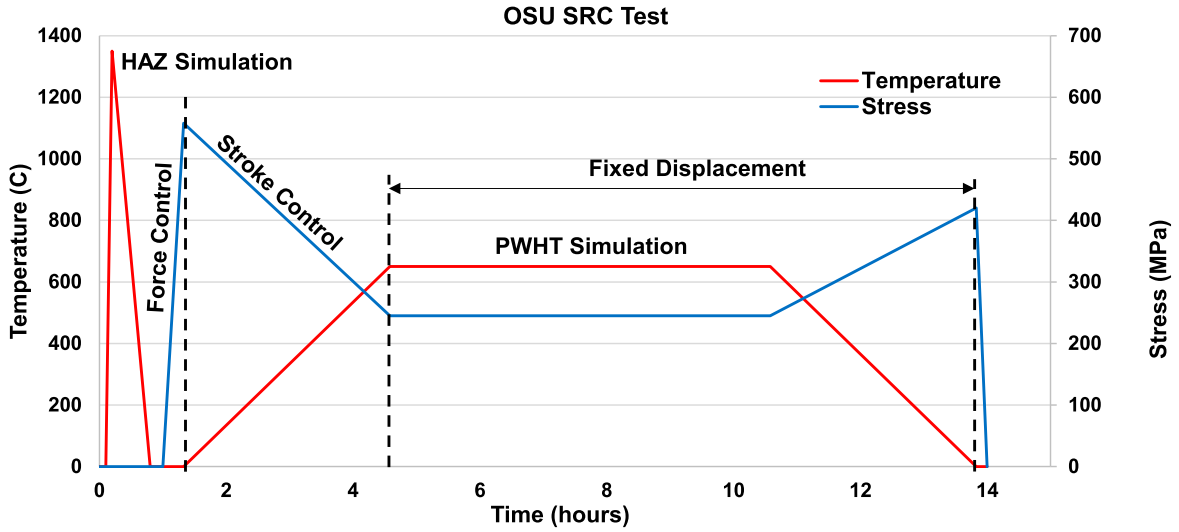

Figure 1. OSU SRC test procedure.

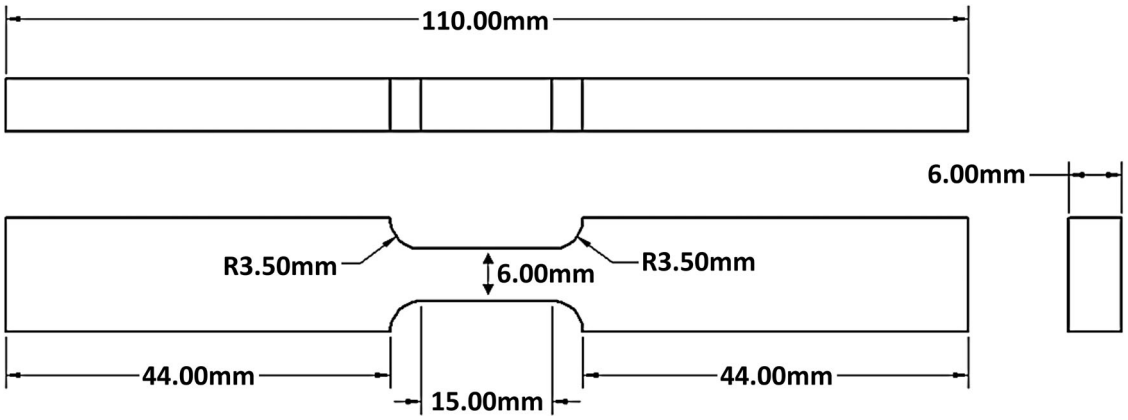

Figure 2. OSU SRC test sample design.

upon reaching the PWHT temperature, i.e. 90% of the elevated temperature yield strength. After reaching the PWHT temperature, the sample is held under fixed displacement to simulate a high level of weld restraint for the test duration, typically 6 h. If an SRC failure does not occur within the PWHT duration, the sample is free cooled to room temperature under fixed displacement and unloaded. This SRC test procedure replicates the worst-case conditions for SRC: welding residual stresses close to material's yield strength and highly restrained weldment subjected to local PWHT.

The local strain in the sample gauge section is measured with digital image correlation (DIC). A full description of the DIC procedure is provided elsewhere [14]. The SRC test sample design utilises a gauge section with square cross-section to allow for two-dimensional DIC strain analysis (Figure 2). The application of DIC allowed quantifying the local strain distribution, the rate of strain accumulation, and the mechanical energy sustained by the tested materials. The strain rate was calculated using the total strain accumulated within the fixed displacement at PWHT temperature portion of the test and the time to failure or the whole test duration, respectively, for SRC susceptible and SRC resistant materials. The density of sustained mechanical energy (SME), within the 6 mm long central portion of the gauge section, was calculated by integrating the stress–strain curves, as shown in Figure 5, which cover the duration of PWHT under fixed displacement. Mechanical energy has been previously used for quantification of fatigue life in low alloy steels [15] and susceptibility to ductility deep cracking in Ni-based alloys [16].

The SRC susceptibility in the OSU test is quantified using the test outputs: time to failure, stress at failure, local strain at failure, reduction in area, and SME. The effectiveness of PWHT, in terms of stress relief in non-failed samples, is quantified by the level of stress reduction both during holding at fixed displacement and at room temperature before and after PWHT simulation. Scanning electron microscopy is performed on fracture surfaces of failed samples for failure mechanism verification. Samples that do not fail in the SRC test are cross-sectioned and examined for microcracks.

Table 2. Chemical composition of tested material, wt-%.

	Grade 11 Heat 1	Grade 11 Heat 2	Grade 11 Weld metal	Grade 22
Al	0.033	0.035	0.0092	0.042
As	0.004	0.001	0.0022	0.005
B	0.0001	0.0001	0.0001	0.002
C	0.14	0.14	0.12	0.156
Cr	1.134	1.43	1.143	2.093
Cu	0.17	0.1	0.057	0.185
Mn	0.45	0.44	0.8446	0.53
Mo	0.54	0.61	0.524	0.927
Nb	0.001	0.001	0.001	0.006
Ni	0.13	0.08	0.054	0.145
P	0.007	0.005	0.0069	0.008
S	0.007	0.001	0.00552	0.01
Sb	0.003	0.001	0.0003	0.011
Si	0.55	0.56	0.1709	0.225
Sn	0.008	0.005	0.0008	0.01
Ti	0.002	0.003	0.0023	0.002
V	0.004	0.004	0.0039	0.005
MPC7 $<$ 0.76	0.794	0.655	(0.221)	NA

Table 3. SRC loading parameters.

SRC test loading parameters	Grade 11 CGHAZ & WM	Grade 22 CGHAZ
YS at 20°C, MPa	620	680
Applied tensile stress at 20°C, MPa (90% YS)	558	612
YS at 650°C, MPa	≈ 230–240	≈ 300–310
Target tensile stress at 650°C, MPa (90% YS)	210	280
Compensation stroke to 650°C, mm	0.25	0.20
Compensation stroke rate to 650°C, μm/°C	0.381	0.317
Compensation stroke 600°C, mm	0.23	0.18
Compensation stroke 691°C, mm	0.27	0.21

Materials and procedure

Low alloy Cr–Mo creep-resistant steels were used for the SRC test demonstration and validation. These included simulated CGHAZs in one heat of Grade 22 steel (HAZ22) and two heats of Grade 11 steels, HAZ11-1 and HAZ11-2, and a submerged arc weld metal in Grade 11 steel, WM11. The chemical composition of the tested materials is shown in Table 2 along with the composition-based Materials Property Council parameter (MPC7) for SRC susceptibility. The MPC7 parameter [2], developed specifically for Grade 11 HAZ, identifies HAZ11-1 as susceptible and HAZ11-2 as resistant to SRC.

The SRC susceptibility in HAZ11-1, HAZ22, and WM11 was evaluated at 600°C, 650°C, and 691°C using the OSU SRC testing procedure defined above. The HAZ11-2 was tested at 650°C. The CGHAZ samples utilised the design shown in Figure 2. The CGHAZ simulations were carried out by heating test samples to 1350°C at a rate of 100°C s^{-1} followed by free cooling to room temperature, which provided cooling time between 800°C and 500°C in the order of 20 s. The WM11 samples were extracted from a 17-pass, 8-layer submerged arc V-groove weldment in the as-welded conditions and used the geometry shown in Figure 3. This was a 1-inch-thick plate, 0.5-inch root, 30° included angle joint welded using the following submerged arc welding procedure: 167°C preheat and 250°C interpass temperatures, AC current of 475 A, 27 V, 110 cm min^{-1} wire feeding rate, and 36.7 cm min^{-1} travel speed.

The SRC loading parameters for the tested materials are detailed in Table 3. The yield strength of all tested materials was determined by tensile testing at room temperature and at 650°C. The compensation stroke values and stroke rates, needed to achieve targeted tensile loads equivalent to 90% of the 650°C yield strength, were determined experimentally by straining test samples at 650°C. The compensation stroke values for the 600°C and 691°C tests were calculated, extrapolating the respective stroke values and rates for 650°C.

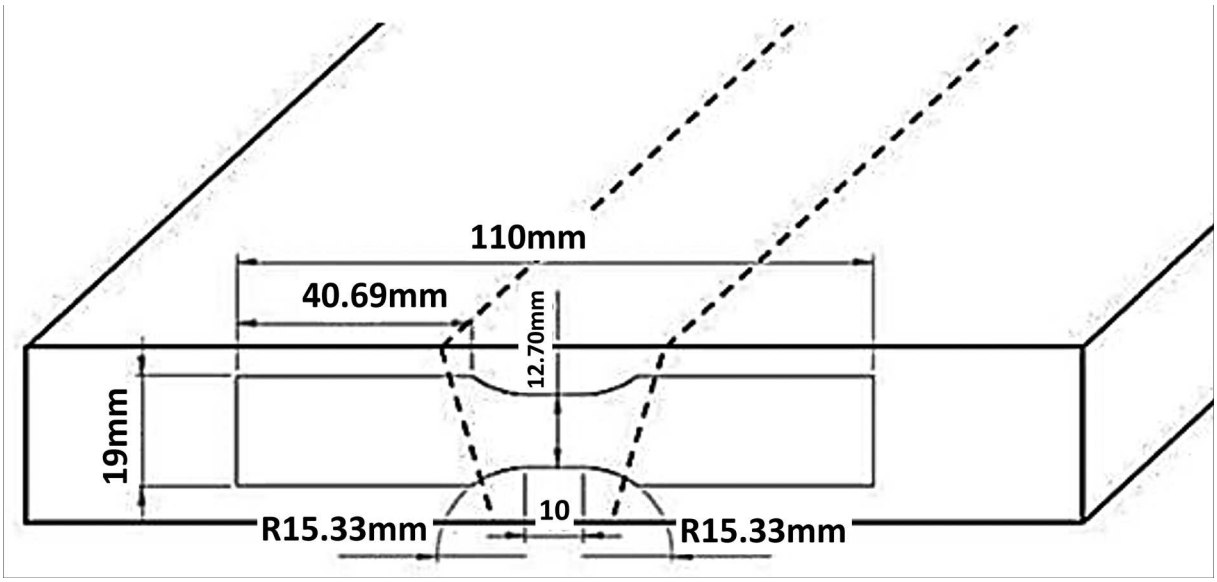

Figure 3. Grade 11 weld metal sample design (sample thickness is 6 mm).

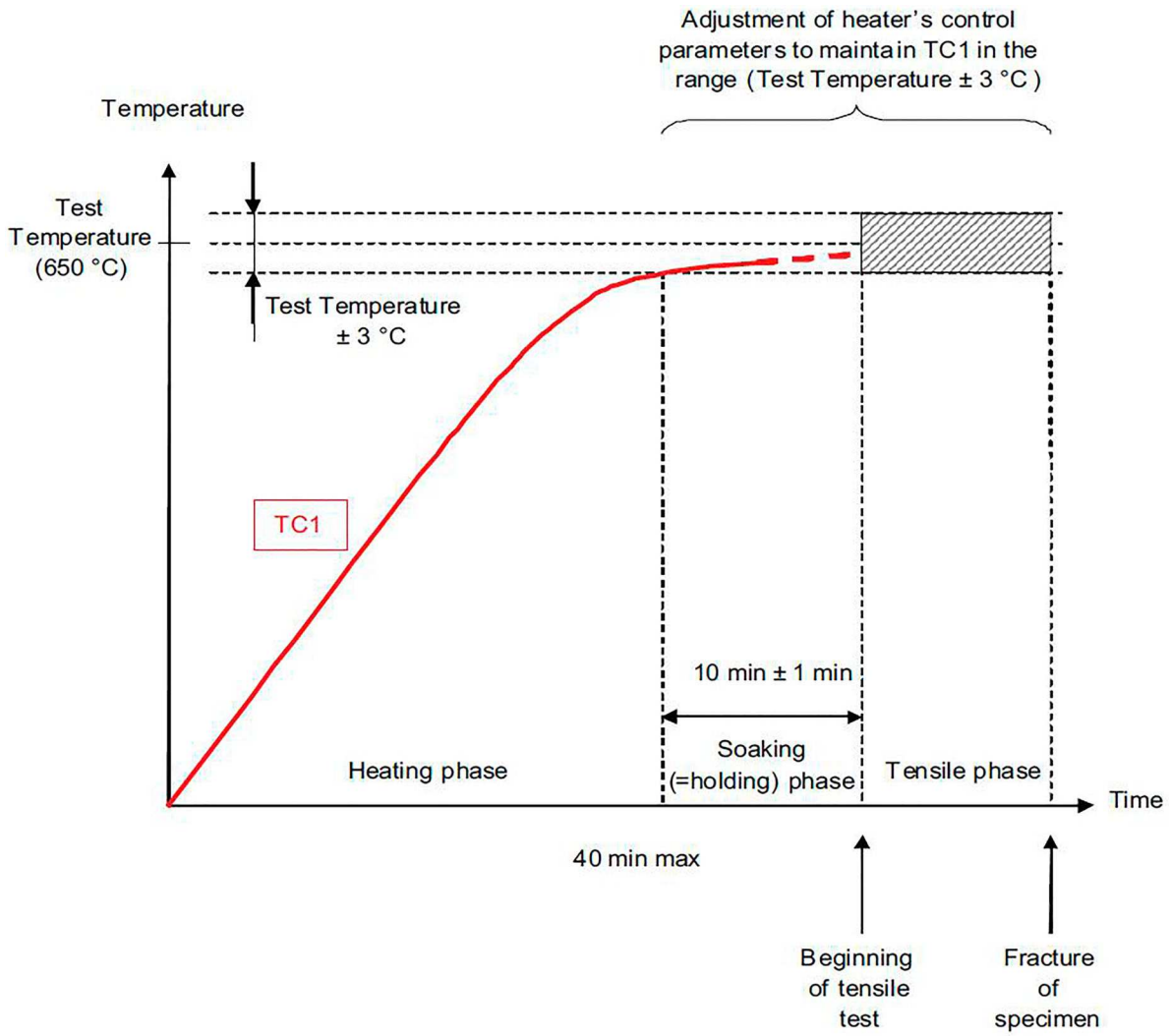

Figure 4. API SRC test schematic of test procedure [10].

Table 4. OSU SRC test results.

Tested material	Test temp, °C	RT stress, MPa	RT strain, %	PWHT start Stress, MPa	PWHT start Strain, %	Time to failure, min	Stress at failure, MPa	Strain at failure, %	RA, %	PWHT end stress, MPa	PWHT end strain, %	Final RT stress, MPa
WM11	600	558	No DIC	305	No DIC	NF*	–	–	–	223	No DIC	497
	650		0.36	236	2.77	NF	–	–	–	82	6.05	367
	691		No DIC	140	No DIC	NF	–	–	–	49	No DIC	279
HAZ11–2	650	558	0.20	216	1.53	NF	–	–	–	131	3.72	541
HAZ11–1	600	558	0.21	297	1.30	103.8	299	1.61	< 1	–	–	–
	650		0.30	200	1.62	63.3	168	2.81	1.1	–	–	–
	691		0.22	On-heating failure 684 °C	−1.7	171	2.72	< 1	–	–	–	
HAZ22	600	612	0.24	323	1.15	238.2	308	1.89	< 1	–	–	–
	650		0.38	279	1.87	52.3	143	3.42	3.6	–	–	–
	691		0.28	174	1.75	108.4	107	4.87	3.8	–	–	–

*No failure.

Comparative study with the API test

The strain to failure SRC test described in API 934A Annex B [10] (API test) is a hot ductility test developed with the goal of quickly screening 2.25Cr-1Mo-V submerged arc weld metal for risk of SRC [17,18]. Average RA of 32% and min. 29% RA is considered as acceptable SRC resistance. The API testing procedure is summarised in Figure 4. This test is currently used and relied upon by industry and, therefore, was selected for comparison to the OSU SRC test.

This study utilised the Gleeble™ thermo-mechanical simulator for API testing of SRC susceptibility in the three heat-affected zones and WM11. Unrestrained samples were heated within 30 min to 650°C and held at temperature for a 10-min soaking period. The samples were then strained to failure at a rate of 0.8 mm min^{-1}.

Table 5. Quantitative parameters of stress relief behaviour and SRC susceptibility.

Tested material	Test temp, °C	Time to failure, min	RA, %	PWHT strain absorption, %	PWHT average strain rate, s^{-1}	PWHT stress relaxation, MPa	PWHT SME, MJ m^{-3}	Total stress relief, MPa
WM11	600	NF*	–	No DIC	–	82	No DIC	61
	650	NF	–	3.28	1.52 10^{-6}	154	4.85	191
	691	NF	–	No DIC	–	91	No DIC	279
HAZ11-2	650	NF	–	2.19	1.01 10^{-6}	85	3.84	17
HAZ11-1	600	103.8	< 1	0.31	4.98 10^{-7}	−2	0.93	
	650	63.3	1.1	1.19	3.13 10^{-6}	32	2.19	
	691	−1.7	< 1	2.72				
HAZ22	600	238.2	< 1	0.74	5.18 10^{-7}	15	2.45	
	650	52.3	3.6	1.55	4.94 10^{-6}	136	2.78	
	691	108.4	3.8	3.12	4.78 10^{-6}	167	3.78	

*No failure.

Table 6. Comparison of API to OSU SRC test results at 650°C.

	RA, %				Strain rate, s-1		SME (MJ m^{-3})	
Sample type	API	OSU	API UTS, MPa	OSU stress at failure, MPa	API	OSU	API	OSU
WM11	73.2	NF*	332	NF	5 10^{-4}	1.52 10^{-6}	No DIC	4.85
CGHAZ11-2	46.3	NF	443	NF		1.01 10^{-6}		3.84
CGHAZ11-1	10.3	1.8	413	120		3.13 10^{-6}		2.19
CGHAZ22	25.7	3.6	425	184		4.94 10^{-6}	90.79	2.78

*No failure.

RA in tested samples is used as a criterion for the determination of SRC susceptibility.

Results

In this study, the OSU test was demonstrated at worst-case conditions for SRC: close to yield strength simulated welding residual stress and high weldment restraint simulated by fixed displacement. Table 4 shows the test results. The strain values were obtained from a 6 mm digital DIC extensometer and represent the average longitudinal strain in the centre of test samples. Quantifiable parameters of the stress relief behaviour and SRC susceptibility are summarised in Table 5. These include time to failure and reduction in area, and strain accumulation, average strain rate, stress relaxation and SME under fixed displacement at PWHT temperature. The total level of stress relief in non-failed samples, calculated as a difference in stress before and after PWHT, is also presented. The WM11 and HAZ11-2 did not fail in the SRC test. The HAZ11-1 sample intended for testing at 691°C failed during heating. The rest of HAZ11-1 and all HAZ22 test samples failed during holding at PWHT temperature. The results from the API test, in terms of RA, stress at failure, and SME, are summarised and compared to the OSU test results in Table 6. WM11 and HAZ11-2 passed, while HAZ11-1 and HAZ22 failed the API RA criterion.

Figure 5 shows the stress–strain curves of all tested materials at PWHT temperature under the fixed

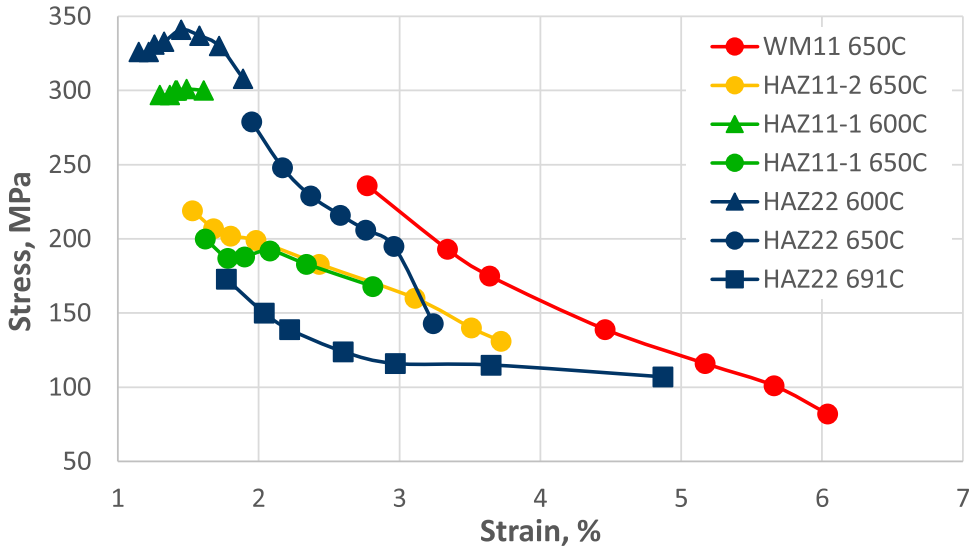

Figure 5. Stress vs. strain curves at PWHT temperature under fixed displacement.

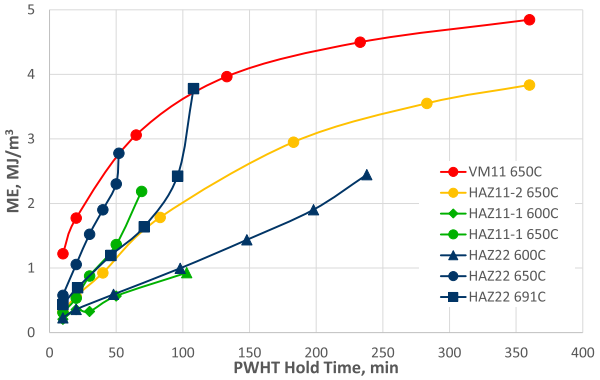

Figure 6. Sustained mechanical energy vs. time at PWHT temperature under fixed displacement.

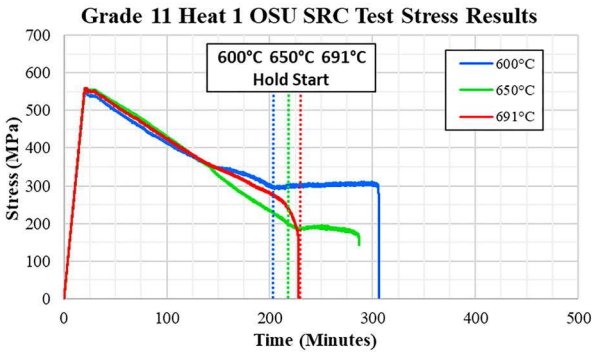

Figure 9. Grade 22 stress vs. time curves at 600°C, 650°C, and 691°C tests.

displacement. The SME, calculated by integration of the strain-curves, is plotted vs. time in Figure 6. Figures 7 and 8 show stress and strain vs. time data for the entire test duration in all materials tested at 650°C. Figures 9–12 show stress and strain vs. time data for HAZ11-1 and HAZ22 at all test temperatures.

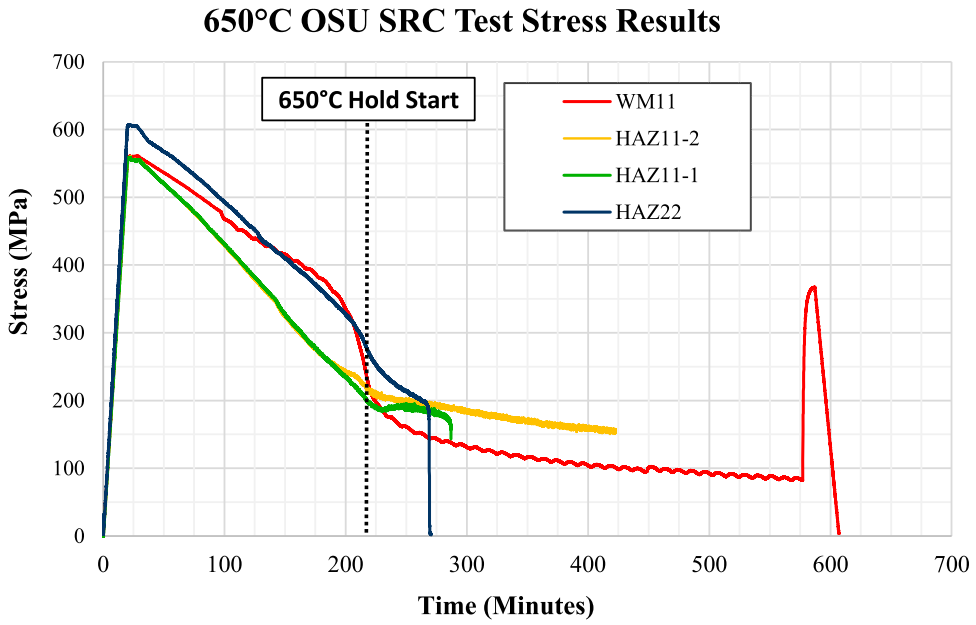

Figure 7. Stress vs. time curves for all materials tested at 650°C.

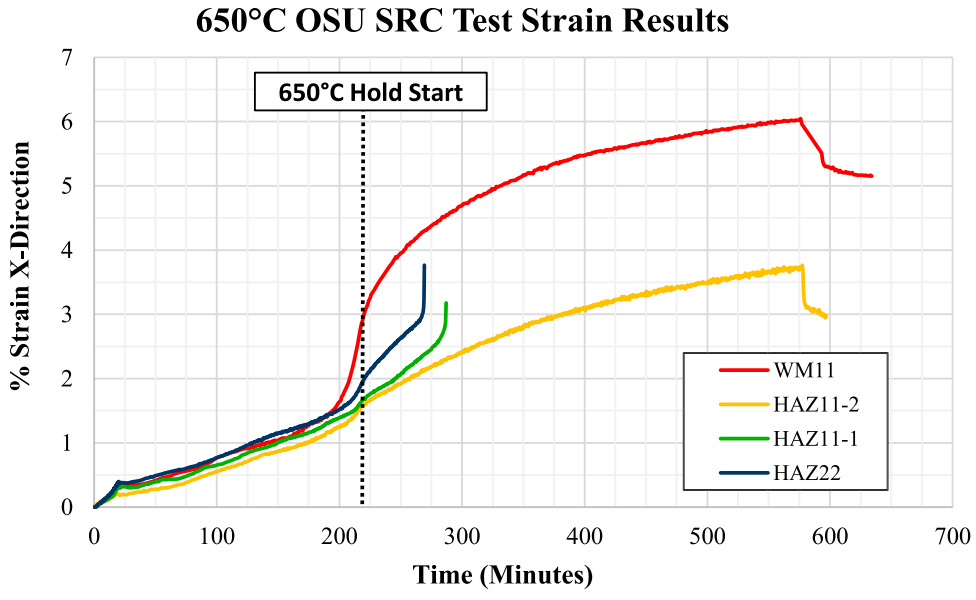

Figure 8. Strain vs. time curves for all materials tested at 650°C.

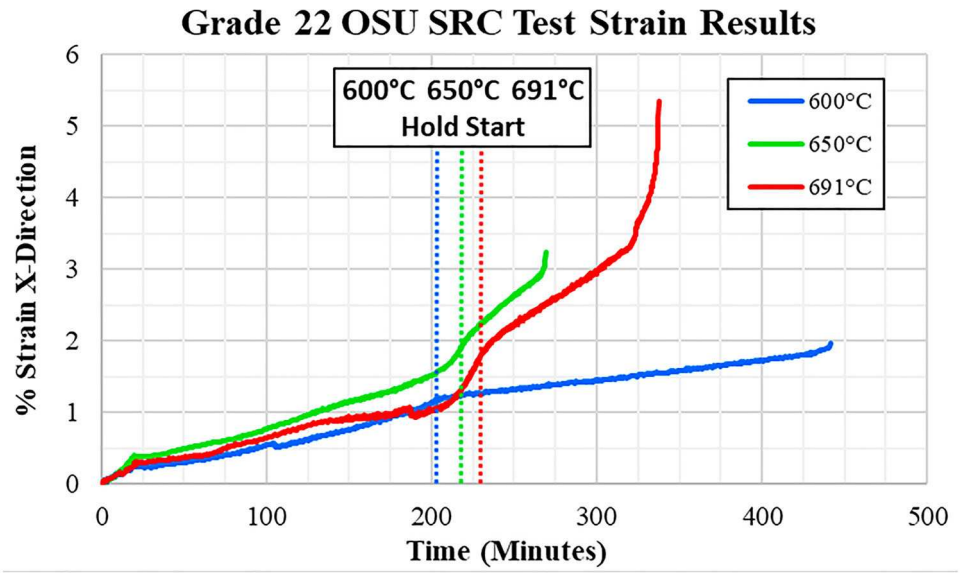

Figure 10. Grade 22 strain vs. time curves at 600°C, 650°C, and 691°C tests.

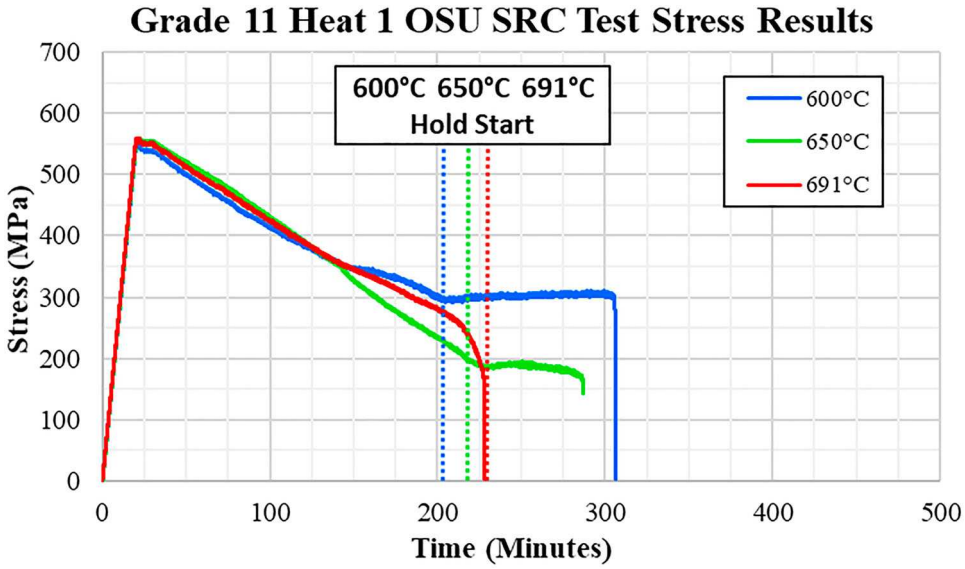

Figure 11. Grade 11 Heat 1 stress data for the 600°C, 650°C, and 691°C OSU SRC Test.

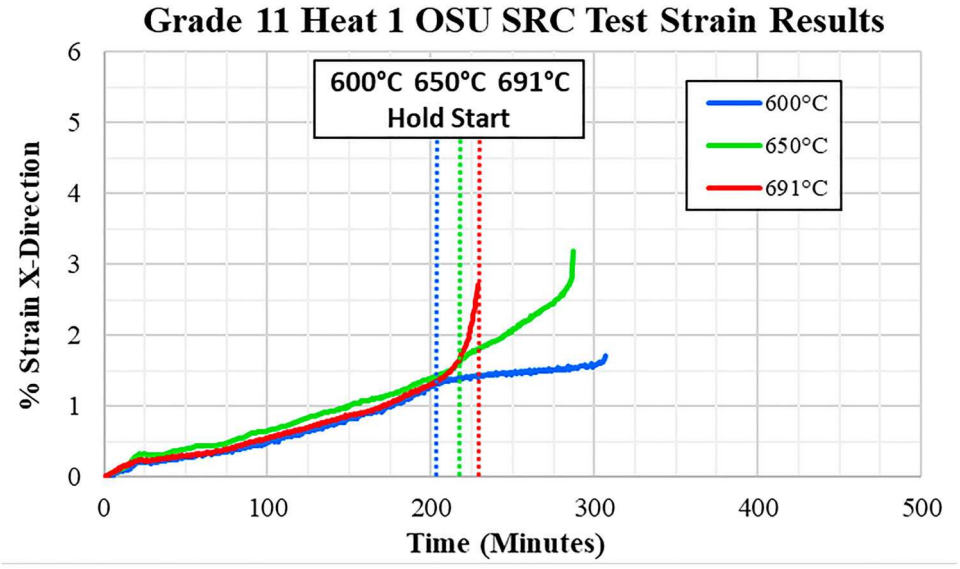

Figure 12. Grade 11 Heat 1 strain data for the 600°C, 650°C, and 691°C OSU SRC Test.

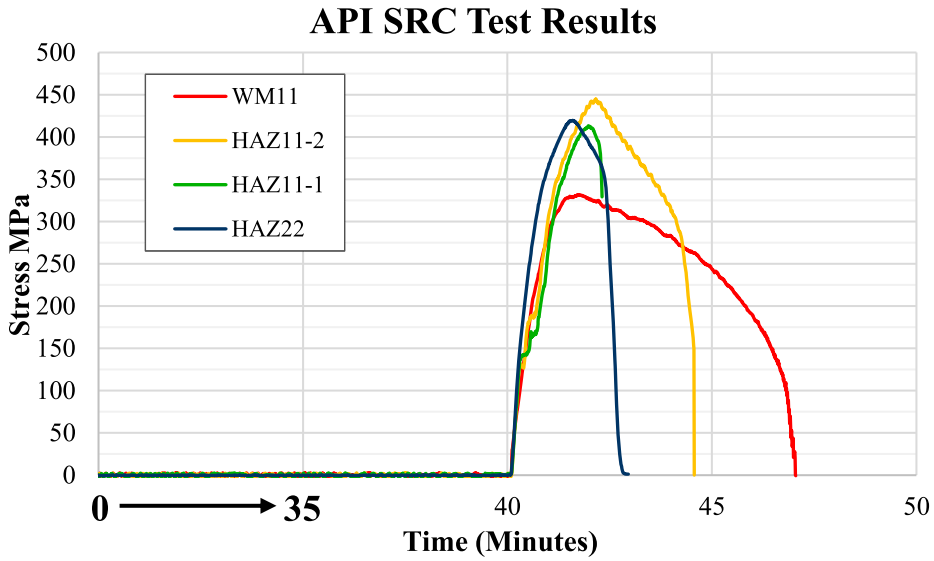

Figure 13. API SRC test results for all tested materials.

The results from the API test are summarised in Figure 13.

Figures 14–17 illustrate the strain distribution maps and kinetics of strain absorption across the entire gauge section of HAZ22 and WM11 samples during holding at 650°C. A strain distribution map in the gauge section of HAZ22 API test sample is shown in Figure 18. Figure 19 compares the strain distribution normal to the restraint direction in HAZ22 samples tested with the OSU and API tests. Figure 20 compares the stress vs. strain curves in these two tests.

The microstructure next to the fracture surface of HAZ22 OSU test sample is shown in Figure 21. The fracture surfaces of OSU test HAZ11-1 sample and the API test HAZ22 sample are compared in Figure 22.

Discussion

The proposed SRC testing procedure has several key advantages over the existing tests listed in Table 1. Compared to the BWI, API, and Lehigh 2015 tests, it applies a tensile load to the test sample on heating, aiming to replicate the effect welding residual stresses have on carbide precipitation and SRC susceptibility before reaching the PWHT temperature. It was shown that heating under tensile load affects the carbide precipitation mechanism [19] and may cause SRC failures in highly susceptible materials, which was experienced both in this work and in previous research [12]. Compared to the Lehigh 2000 and OSU 2014 procedures, the controlled straining on heating to PWHT temperature compensates the effect of thermal expansion on the applied tensile load and allows evaluating the effect of residual stress level on SRC susceptibility. Additionally, the implementation of DIC allows for studying the strain accumulation kinetics in the process of stress relaxation and for accurate quantification of the local strain level and SME leading to SRC failures.

The quantitative outputs of the OSU test clearly differentiated SRC susceptibility in the tested materials, Table 5. WM11 can be classified as the most resistant to SRC, based on no-failure for the 6-h test duration at the three test temperatures. Compared to the other tested materials, WM11 exhibited higher levels of strain accumulation, stress relaxation, and SME for the fixed displacement at the PWHT temperature portion of the test. On heating to PWHT temperature of 650°C, the WM11 sample was overloaded above the 210 MPa targeted stress (Tables 3 and 4) due to a random stroke drift. As a result, accelerated stress relaxation and strain accumulation started on the heating before reaching 650°C (Figures 7 and 8). The lack of failure, even when loaded above yield strength at the test temperature, demonstrates high resistance to SRC of WM11. HAZ11-2 also passed the test at 650°C, but with lower values of the SRC susceptibility parameters.

The two materials that failed the SRC test, HAZ11-1 and HAZ22, have different chemical compositions and mechanical properties, which would influence the kinetics of carbide precipitation, grain interior strengthening, strain accumulation, and stress relaxation during PWHT. Compared to HAZ11-2, the higher yield strength and content of carbon and carbide formers in HAZ22 would, respectively, lead to a higher level of welding residual stress and a higher degree of grain interior strengthening during PWHT. Nevertheless, HAZ22 performed better than HAZ11-1 in the OSU SRC test, based on higher RA, strain absorption, levels of stress relaxation, and SME, Table 5. Except for the 650°C test, HAZ22 also exhibited longer times to failure than HAZ11-1.

The OSU test reproduced the brittle intergranular fracture morphology with micro-ductility features, typically found in SRC of Cr-Mol steels [6,17,20–22]. Secondary cracks along primary austenite grain boundaries (PAGBs), oriented normal to 45° relative to the

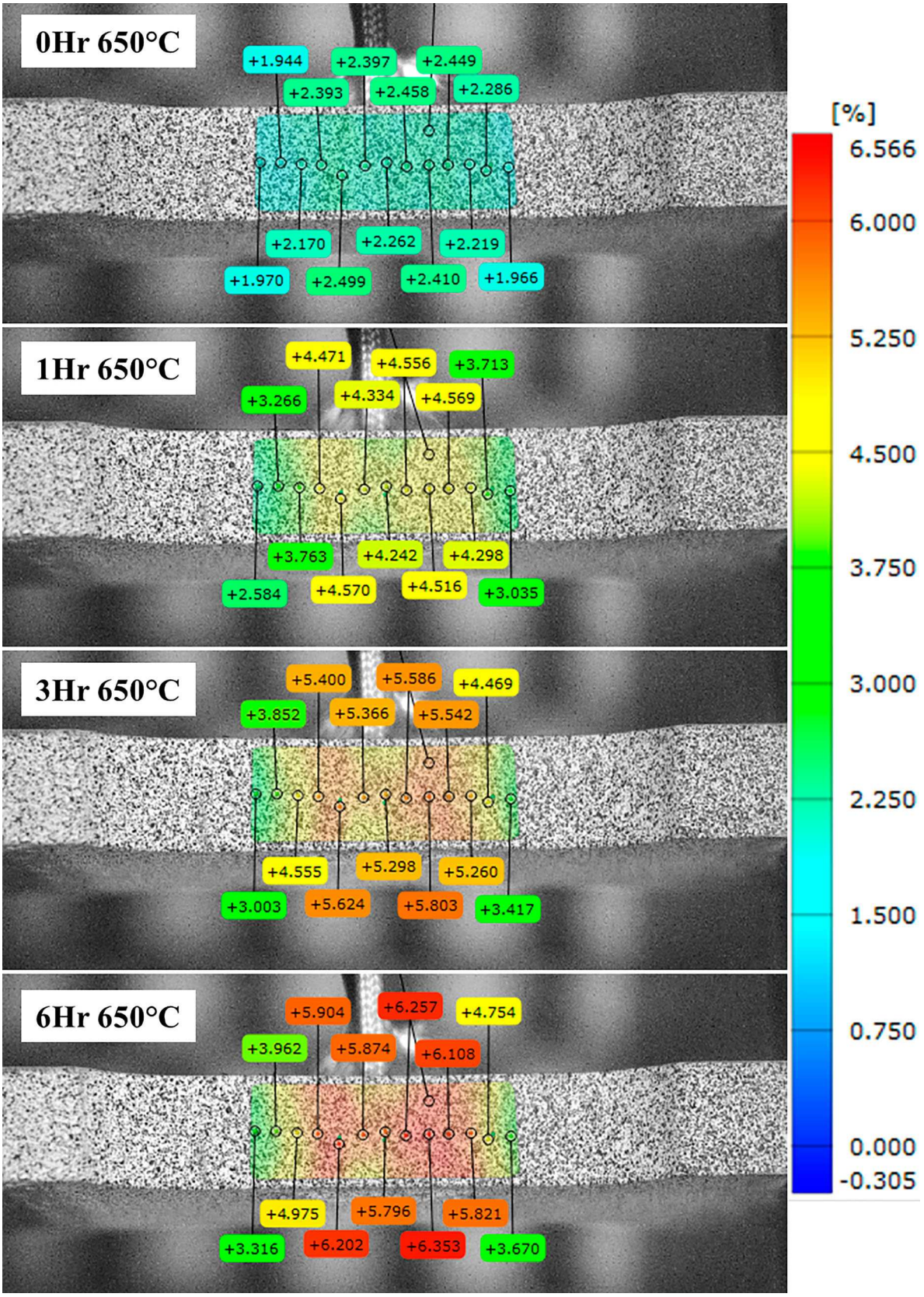

Figure 14. Gauge section DIC strain maps in OSU test sample of WM11.

direction of restraint generated tensile stress, were found near the intergranular fracture surface in HAZ22 sample tested at 650°C (Figures 21(a,b)). Evidence of void nucleation along PAGBs and crack formation at PAGB triple points were also identified (Figure 21(c)). The fracture surface of the HAZ11-1 sample tested at 650°C exhibited brittle intergranular morphology with micro-ductility features (Figure 22(a)).

The SRC susceptibility rankings generated by the OSU test correlate well with the composition-based

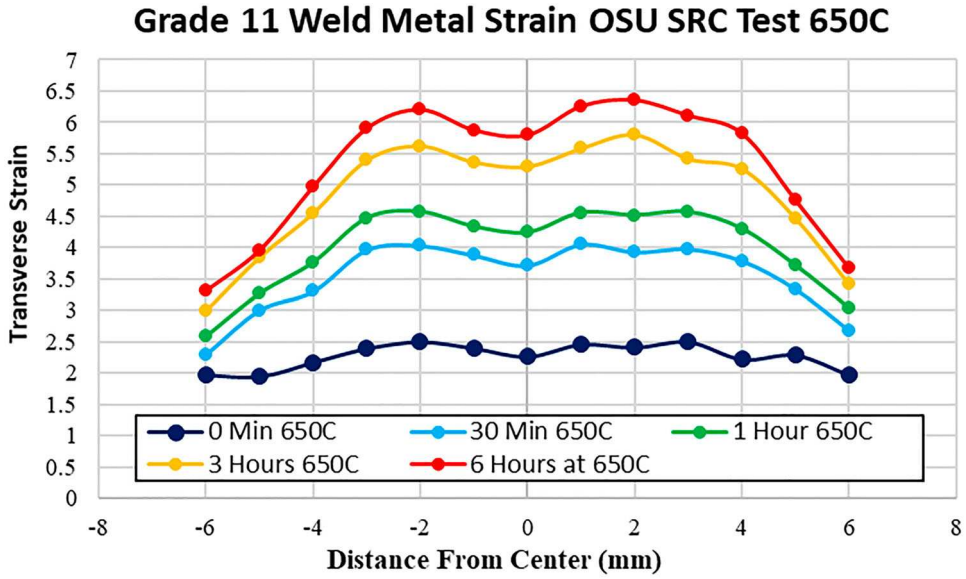

Figure 15. Strain absorption in the gauge section in OSU test sample of WM11.

cracking susceptibility parameter (Table 2). The MPC7 identifies HAZ11-1 as susceptible to SRC and WM11 more resistant than HAZ11-2. There is also a full correlation of the SRC rankings generated by the API and OSU tests (Table 6). WM11 passed the API test with significantly higher reduction in area than HAZ11-2. HAZ11-1 failed that test with a lower reduction in area than HAZ22.

The results of this study show the API test does not completely replicate the SRC mechanism in Cr–Mo steels. For the studied cases, the strain rate of API test is two orders of magnitude higher than the average rate of strain accumulation under fixed displacement in the OSU test (Table 6). It generates a typical high-temperature tensile test stress–strain curve with a mechanical energy factor of thirty higher than SME in the externally restrained OSU test (Figure 20). Compared to the OSU test (Figures 16 and 17), the API test produces: (1) more uniform strain distribution and lower degree of strain concentration before necking, and (2) very high tensile and compressive strains before failure (Figures 18 and 19). These are indicators for a lower degree of grain boundary embrittlement and dominating ductile failure mechanism, which correlates with the mixed intergranular and ductile fracture morphologies in Figure 22(b). The specifics of the API test resulted in significantly higher RA, stress at failure and elongation at failure values compared to the OSU test (Table 6 and Figures 13 and 20).

Results from the OSU SRC test can guide materials selection, welding and PWHT procedure optimisation for effective stress relief and mitigation of SRC in welds of Cr–Mo steels. A PWHT at 691°C would effectively reduce welding residual stresses in WM11 without risk of SRC, while stress relief at 650°C would not be effective for HAZ11-2(Table 5). Testing HAZ11-1 and HAZ22 at lower stress levels can demonstrate if optimising welding procedures for residual stresses reduction could mitigate SRC in these materials. The degree of stress relaxation in HAZ22 increases with rising the PWHT temperature. Therefore, PWHT at 691°C is expected to provide effective stress relief in case SRC susceptibility in this material is mitigated by lowering welding residual stresses. HAZ11-1 failed on heating to 691°C PWHT, showing that PWHT at 650°C could be more effective for stress relief at lower residual stress levels.

The SRC phenomenon can be analyzed as a product of two competing processes: stress relaxation vs. simultaneous grain boundary strain accumulation and embrittlement. Stress relaxation in the SRC temperature range occurs predominantly by a comparatively slow dislocation creep mechanism and plastic strain [3,23–25]. The grain boundary strain accumulation results from grain interior strengthening by precipitation of secondary carbides [2,3,6,23,26]. It was demonstrated that carbide precipitation in Cr–Mo steels is a fast process that can initiate heating during PWHT [14,19]. Grain boundary embrittlement results from diffusion-controlled segregation of impurities and tramp elements and precipitation of coarse carbides [2,3,6]. The quantitative outputs of the OSU test can help better understand the complex interaction kinetics of these processes and their effect on SRC and stress relief in welds of creep-resistant alloys.

In the SRC susceptible materials, the process of grain interior strengthening outpaces the overall stress relaxation, leading to grain boundary strain accumulation and SRC failures. The 600°C stress–strain curves of HAZ11-1 and HAZ22 exemplify extreme conditions for SRC: less than 1% strain accumulation and high stress at failure with insignificant stress relaxation in HAZ22 and slight stress increase in HAZ11-1 (Tables 4 and 5, Figures 5, 9 and 11). The strain accumulation

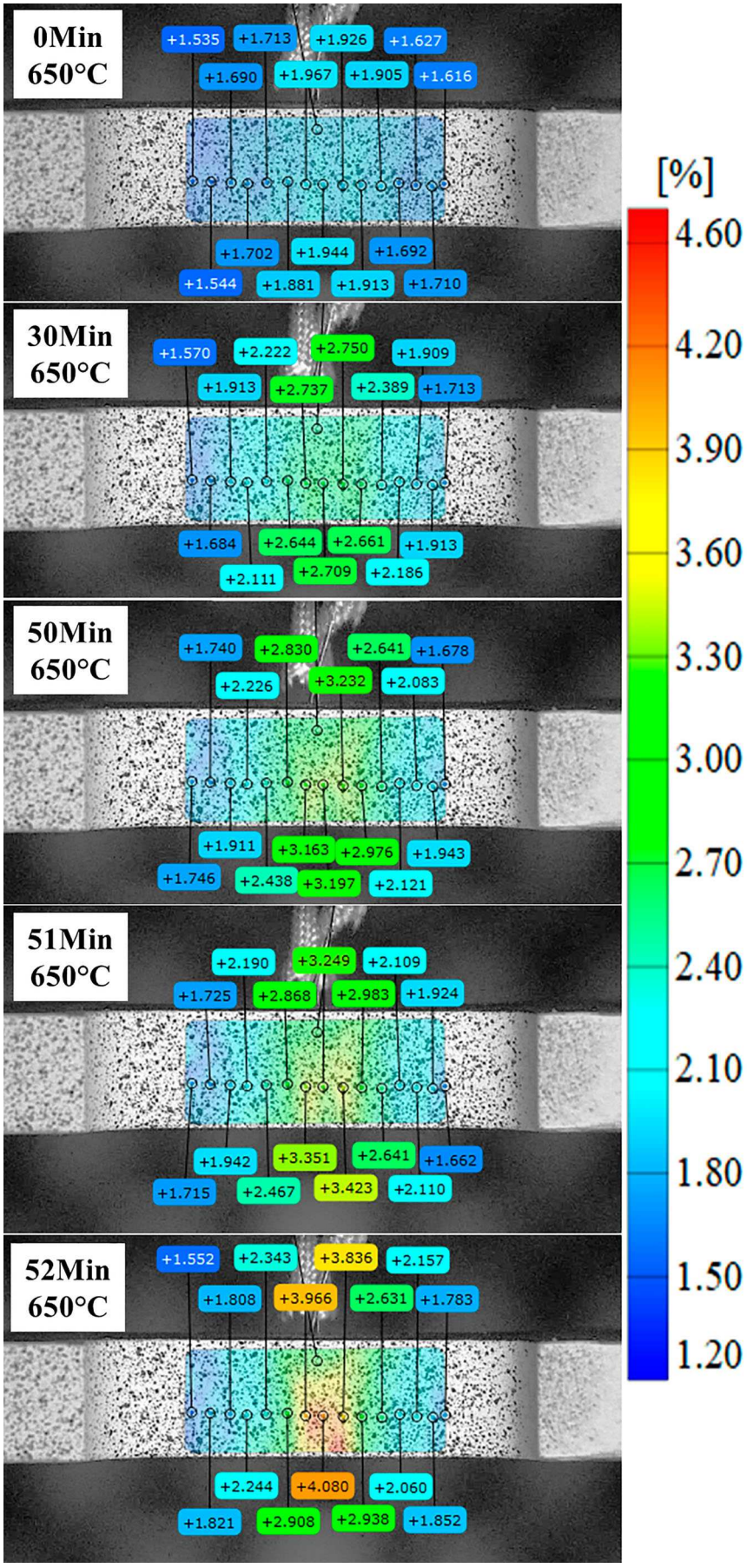

Figure 16. Gauge section DIC strain maps in OSU test sample at 650°C of HAZ22.

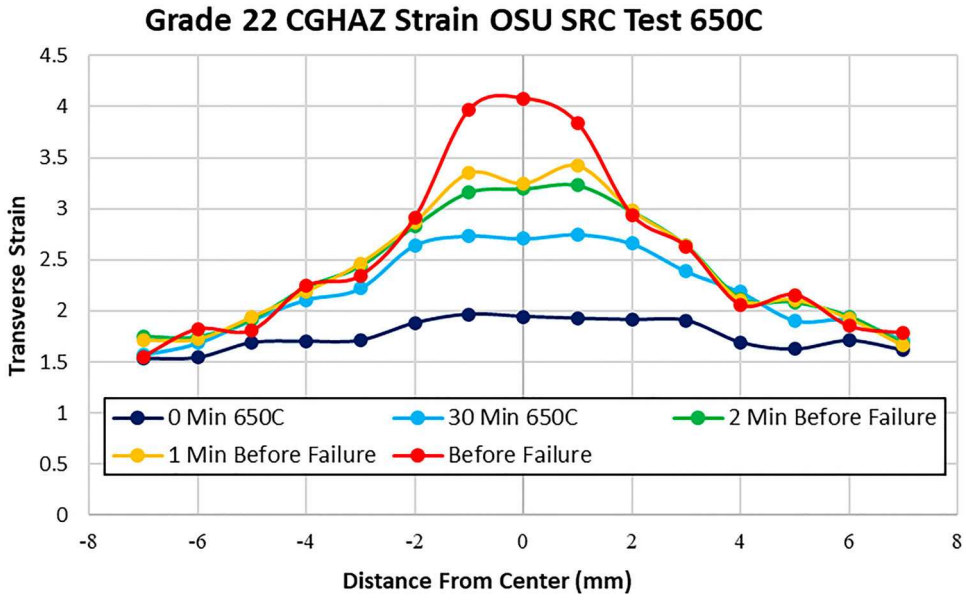

Figure 17. Strain absorption in the gauge section in OSU test sample of HAZ22.

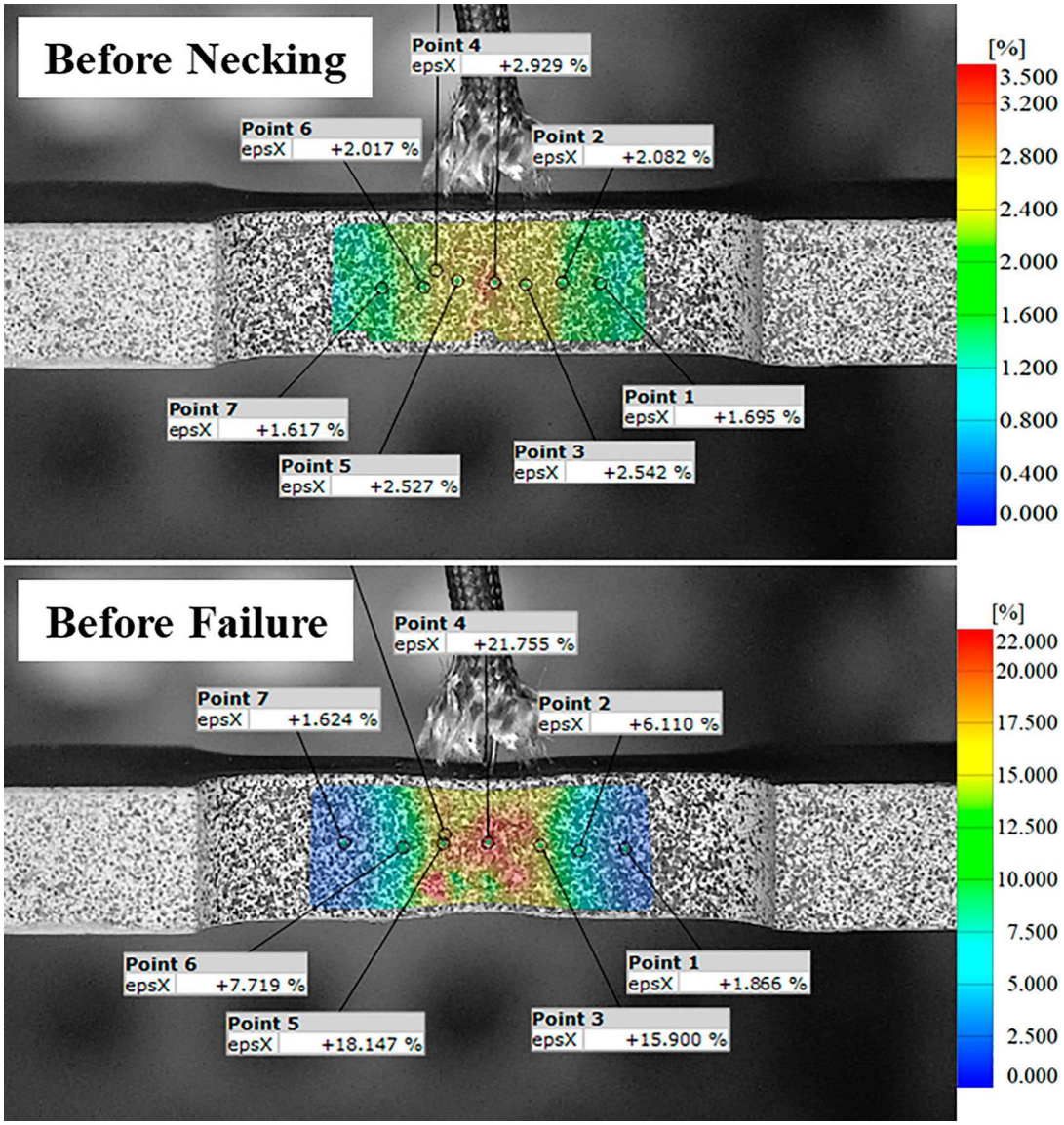

Figure 18. Gauge section strain distribution in API test sample of HAZ22.

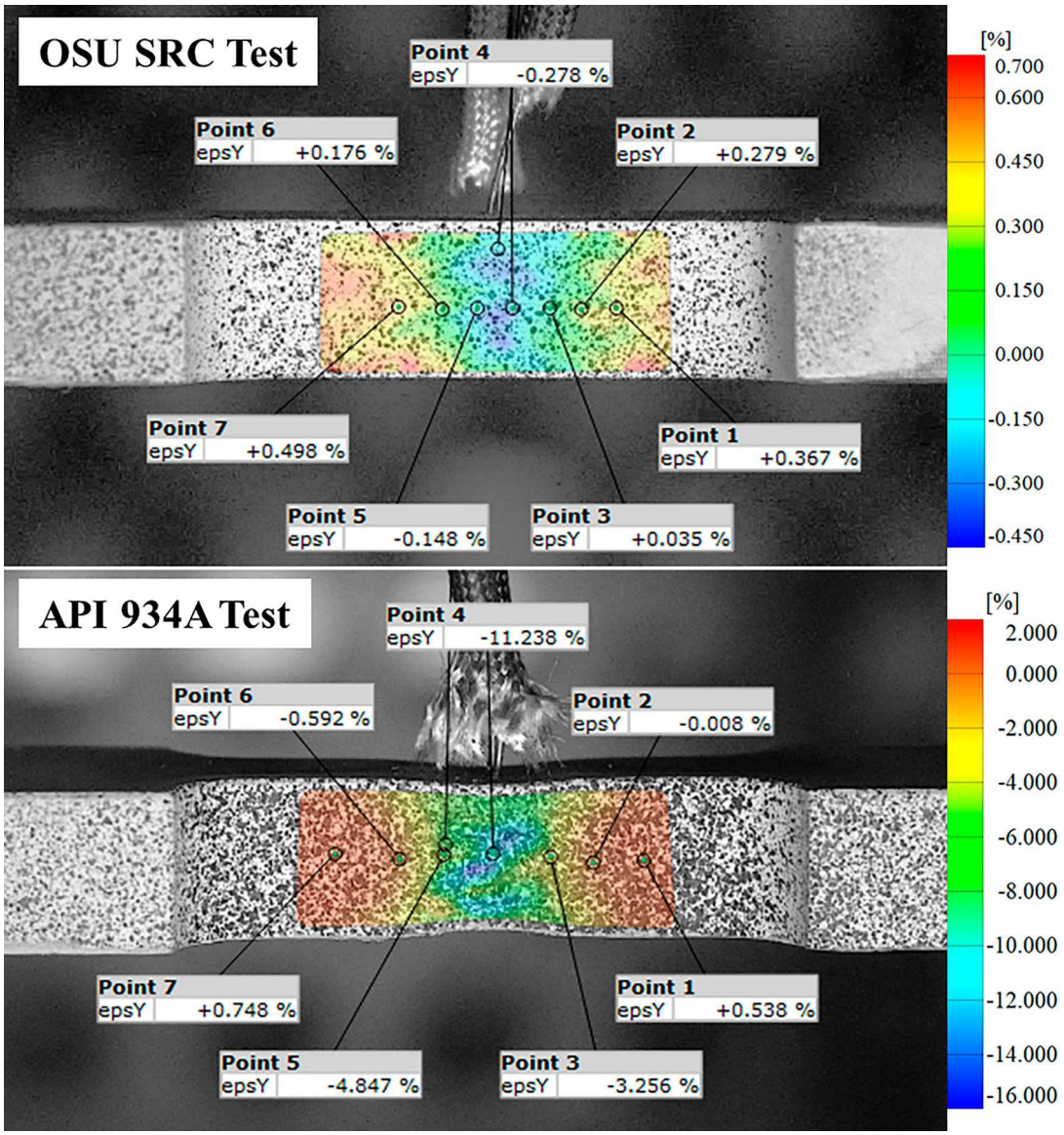

Figure 19. Strain distribution normal to restraint direction in OSU and API test samples of HAZ22.

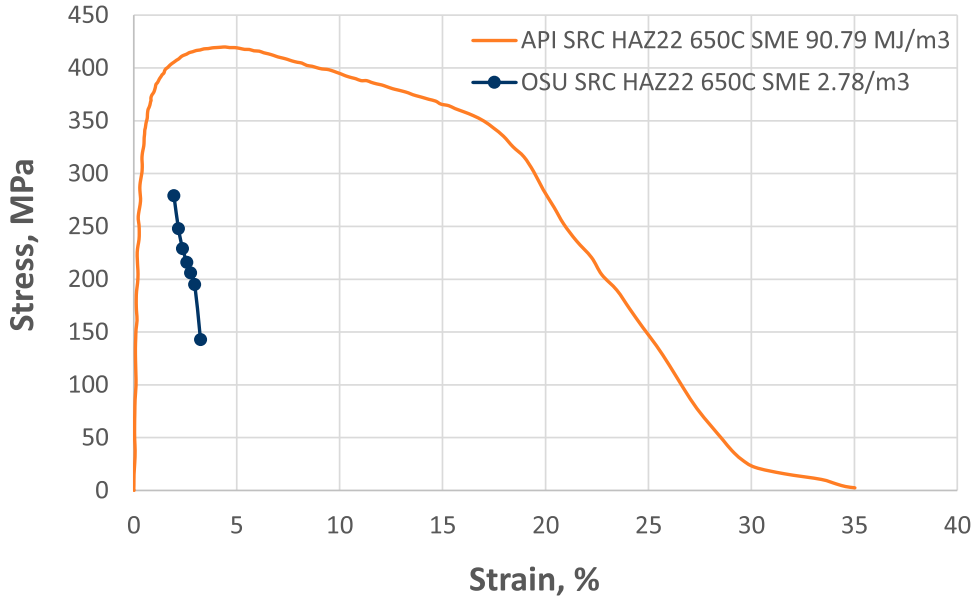

Figure 20. Stress vs. strain curves in the API and OSU SRC tests.

a) Intergranular Failure

b) Secindary cracks at PAGBs

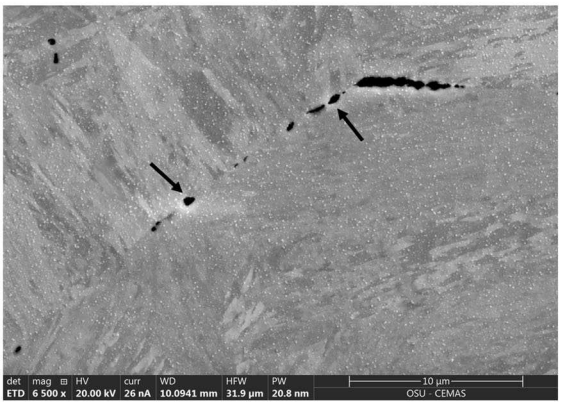

c) Void nucleation along PAGBs

Figure 21. OSU test of HAZ22 sample at 650°C. Intergranular failure (a), secondary cracks and PAGBs (b), voids along PAGBs and crack nucleation at PAGB triple point (c).

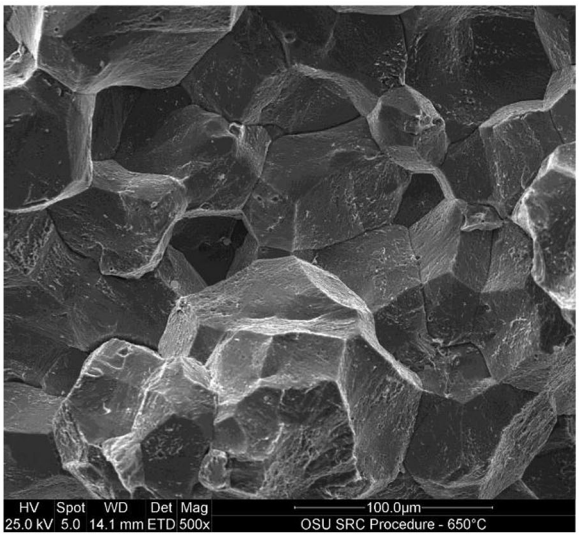

a)

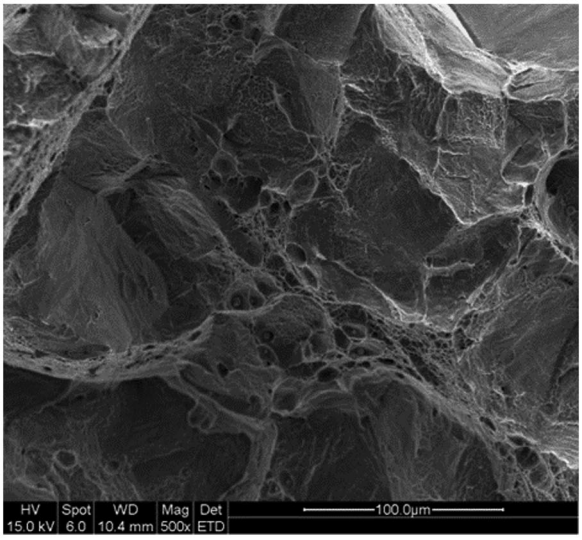

b)

Figure 22. SRC fracture surfaces in Grade 11-1 CGHAZ after testing at 650°C (a) OSU SRC test, (b) API 934A test.

is almost linear with significant acceleration shortly before SRC failure (Figures 10 and 12). The increase in stress during holding at PWTH temperature, about 20 MPa in HAZ22 and 3 MPa in HAZ11-1, is a potential effect of carbide precipitation. A significant stress increase under similar conditions, strain-age cracking test under fixed displacement in precipitation strengthened Ni-base alloys, was related to intensive carbide precipitation [27]. The stress increase under fixed displacement at comparatively low PWHT temperature and high initial stress level can be considered a result of grain interior strengthening kinetics outpacing stress relaxation.

The larger degree of strain accumulation and stress reduction in HAZ11-1 and HAZ22 at 650°C and 691°C indicate faster kinetics of stress relaxation (Figures 5 and 9–12). The shorter times to failure and the accelerated kinetics of strain accumulation in the last stage of stress relaxation before failure evidence faster grain boundary embrittlement kinetics. This is also demonstrated by the steep gradient of strain concentration forming shortly before failure in the gauge section of the HAZ22 sample tested at 650°C (Figures 17 and 18).

The SRC resistant materials, WM11 and HAZ11-2, gradually relieved stresses absorbing strain without failure until the end of PWHT (Figures 7 and 8). This was followed by stresses increase on cooling to room temperature due to thermal contraction under fixed displacement. HAZ11-1 and HAZ11-2 had almost overlapping stress–strain curves, with the latter exhibiting

higher degrees of strain accumulation and stress relaxation (Figure 5). HAZ11-2 had slower kinetics of strain accumulation and faster kinetics of stress reduction, evidencing that the stress relaxation process outpaced grain embrittlement (Figures 7 and 8). WM11 exhibited the fastest kinetics of stress reduction and strain accumulation of all materials tested at 650°C. The uniform strain distribution in the gauge section of this sample, during holding at PWHT temperature, can be attributed to effective stress relaxation by dislocation creep and plastic strain (Figures 14 and 15).

The mechanical energy absorbed by the tested materials during holding at PWHT temperature is also indicative for SRC susceptibility (Table 5 and Figure 6). The SRC susceptible HAZ11-1 and HAZ22 exhibited linear to accelerating kinetics of mechanical energy absorption and lower values of SME compared to the SRC resistant WM11 and HAZ11-2. The results of this study demonstrate that SRC and stress relaxation in case of no SRC, occurring during PWHT under fixed displacement, are low strain – low strain rate – low energy failure mechanisms. The SRC susceptible materials absorbed 0.3–3.1% strain at a rate of 5.10^{-7} to 5.10^{-6} s^{-1} and sustained mechanical energy of 0.9–3.8 MJ m^{-3}. The two SRC resistant materials respectively absorbed 2.2 and 3.3% strain at a strain rate of 1.10^{-6} and $1.5.10^{-6}$ s^{-1} and sustained mechanical energy of 3.84 and 4.85 MJ m^{-3}. In comparison, room temperature tensile test in Grade 22 steel at a strain rate of $1.10^{-3}s^{-1}$ resulted in 43.7% elongation and 205 MJ m^{-3} mechanical energy. The total plastic strain energy of fatigue failure in a low alloy steel ranges from 10^4 to 10^5 MJ m^{-3} [15].

Conclusions

The results of this study demonstrate that the proposed testing procedure replicates the mechanism of stress relief cracking in welds of creep-resistant Cr–Mo steels during PWHT under fixed displacement. Implementation of digital image correlation allows quantifying key parameters of the stress relaxation and stress relief cracking phenomena, including local strain, kinetics of strain accumulation, strain rate, and sustained mechanical energy.

Rankings of the OSU test for susceptible and resistant to stress relief cracking materials correlated well with the composition-based susceptibility parameter MPC7, and with the API test. The OSU test quantifies the level of stress relief in resistant materials and can be used in materials selection and for optimisation of welding and PWHT procedures aiming at effective stress relief and mitigation of stress-relief cracking.

During PWHT under fixed displacement, susceptible to stress-relief cracking materials exhibit lower levels of stress relief, strain absorption, and sustained mechanical energy. Slow stress relief and accelerated strain absorption before failure, related to localised strain concentration, demonstrate that kinetics of interior grain strengthening and grain boundary embrittlement outpace the process of stress relaxation. In contrast, resistant materials exhibit a higher level of stress relaxation and strain absorption with more uniform strain distribution and no failure.

The phenomena of stress relaxation and of stress relief cracking in the tested materials can be characterised as low strain – slow strain rate – low energy processes. Under fixed displacement, the materials susceptible to stress-relief cracking absorbed 0.3–3.1% strain at a strain rate of 5.10^{-7} to 5.10^{-6} s^{-1} and sustained mechanical energy of 0.9–3.8 MJ m^{-3}. The two resistant materials respectively absorbed 2.2% and 3.3% strain at a strain rate of 1.10^{-6} and $1.5.10^{-6}$ s^{-1} and sustained mechanical energy of 3.84 and 4.85 MJ m^{-3}.

Strain to failure tests cannot replicate the stress relaxation and stress relief cracking mechanisms in Cr–Mo steel weldments. While both the externally restrained OSU test and the strain to failure API test can determine susceptibility to stress relief cracking, the OSU test reproduced the typical for stress relief cracking void nucleation and crack propagation along prior austenite grain boundaries and brittle intergranular failure with micro-ductility.

Disclosure statement

No potential conflict of interest was reported by the author(s).

Funding

This research was supported by Shell Global Solutions and Lincoln Electric within the NSF Manufacturing and Materials Joining Innovation Center (Ma^2JIC).

References

[1] Nakamura H, Naiki T, Okabayashi H. Fracture in the process of stress-relaxation under constant strain. 1st International Conference on Fracture, September 1965, Sendai, Japan, Vol. 2; 1965 p. 863–878.
[2] Lundin CD, Liu P, Qiao C Y.P, et al. An experimental study of causes and repair of cracking of 1.25Cr- 0.5Mo steel equipment. Welding Research Council, Bulletin No. 411; 1996.
[3] Nawrocki JG, DuPont J.N, Robino C.V, et al. The mechanism of stress-relief cracking in a ferritic alloy steel. Weld J. 2003;82:25s–35s.
[4] Shin J, McMahon CJ. Mechanisms of stress relief cracking in a ferritic steel. Acta Metall. 1984;32:1535–1552.
[5] Lundin CD, Khan KK. Fundamental studies of the metallurgical causes and mitigation of reheat cracking in $1^1/4$ Cr - $^1/2$ Mo and 2 $^1/_4$ Cr-1Mo steels. Welding Research Council, Bulletin No. 409; 1996.
[6] Heo NH, Chang JC, Kim S-J. Elevated temperature intergranular cracking in heat-resistant steels. Mater Sci Eng A. 2013;559:665–677.
[7] Trent MC. Development and use of a simple test method to evaluate reheat cracking sensitivity in the weld

deposit region of a submerged arc weld [MSc thesis]. University of Tennessee, Knoxville; 2012.
[8] McMahon CJJ, Dobbs RJ, Gentner DH. Stress relief cracking in MnMoNi and MnMoNiCr pressure vessel steels. Mater Sci Eng. 1979;37:179–186.
[9] Dhooge A, Vekeman J. New generation 21/4Cr steels T/P 23 and T/P 24 weldability and high temperature properties. Weld World. 2005;49:75–93.
[10] API 934-A. Materials and fabrication of 2 1/4Cr-1Mo, 2 1/4Cr-1Mo-1/4 V, 3Cr-1Mo, and 3Cr-1Mo-1/4 V steel heavy wall pressure vessels for high-temperature, high pressure hydrogen service. API Recommended Practice, Second Edition; 2008.
[11] Nawrocki JG, DuPont J.N, Robino C.V, et al. The stress-relief cracking susceptibility of a new ferritic steel—part 1: single-pass heat-affected zone simulations. Weld J. 2000;79:355s–362s.
[12] Strader K, Alexandrov B, Lippold J. Stress-relief cracking in simulated-coarse-grained heat affected zone of a creep-resistant steel. In: T. Bollinhaus, J.C. Lippold, C.E. Cross, Editors. Cracking phenomena in welds IV. Berlin: Springer; 2016. p. 475–493.
[13] Kant R, DuPont J. Stress relief cracking susceptibility in high temperature alloys. Weld J. 2019;98:29s–49s.
[14] Sarich C. Stress relief cracking in low alloy creep resistant steels [PhD dissertation]. The Ohio State University; 2021.
[15] Ellyn F, Kujawski D. Plastic strain energy in fatigue failure. J Pressure Vessel Technol. 1984;106:342–347.
[16] Luther S, Alexandrov BT. Recreating ductility-dip cracking via Gleeble based welding simulation. Weld J. 2021;100:27s–39s.
[17] Chauvy C, Pillot S. Prevention of weld metal reheat cracking during Cr-Mo-V heavy reactors fabrication. 2009 ASME Pressure Vessel and Piping Conference. PVP Paper 2009-78144; 2009.
[18] Pillot S, Chauvy C. Standard Reliable Testing Procedure for 21/4Cr-1Mo-V Welding Quality Control & Acceptance – Prevention of SAW Filler Material Reheat Cracking during Fabrication of Heavy Reactors. 2012 ASME Pressure Vessel and Piping Conference. PVP Paper 2012-78030; 2012.
[19] Kromm A, Lausch T, Schröpfer D, et al. Influence of welding stresses on relief cracking during heat treatment of a creep-resistant 13CrMoV steel. part II: mechanisms of stress relief cracking during post weld heat treatment. Weld World. 2020;64:819–829.
[20] Glossop BA, Eaton NF, Boniszewski T. Reheat cracking in Cr–Mo–V steel weldments. Metal Constr Br Weld J. 1969;1969(1):68–73.
[21] Ghiya SP, Bhatt DV, Rao RV. Stress relief cracking in advanced steel material overview. Proceedings of the World Congress on Engineering, 2009, Vol. 2; 2009.
[22] Maitzner CF. Stress relief cracking in weldments. Welding Research Council, Bulletin No. 211; 1975.
[23] Abe F, Kern T-U, Viswanathan R. Creep-resistant steels. Cambridge: Woodhead Publishing; 2008.
[24] Ashby MF. A first report on deformation-mechanism maps. Acta Metall. 1972;20:887–897.
[25] Dong P, Song S, Zhang J. Analysis of residual stress relief mechanisms in post-weld heat treatment. Int J Press Vessels Pip. 2014;122:6–14.
[26] Tamaki K. Effect of carbides on reheat cracking sensitivity. Trans Jpn Weld Soc. 1984;15:8–16.
[27] Lippold JC. Elevated temperature solid State cracking in welds. In: T. Bollinhaus, J.C. Lippold, C. E. Cross, Editors. Cracking phenomena in welds IV. Berlin: Springer; 2016. p. 229–265. ISBN 978-3-319-28434-7.